Materials Advances

Accepted Manuscript

This article can be cited before page numbers have been issued, to do this please use: D. Saha, M. S. Khan, H. A. Gandhi, S. R. Sarah, V. K. Aswal and J. Bhattacharya, *Mater. Adv.*, 2026, DOI: 10.1039/D6MA00049E.

View Article Online
DOI: 10.1039/D6MA00049E

SDS-Induced Structural Transitions of Hemoglobin Revealed by Spectroscopic Techniques and Small-Angle Neutron Scattering

Debasish Saha[†‖], Suhail Khan[‡‖], Harsh A. Gandhi[‡‖], Shafinaz Rahman Sarah[‡], Vinod K. Aswal[†], Jaydeep Bhattacharya[‡,*]

[†]Solid State Physics Division, Bhabha Atomic Research Centre, Mumbai 400085, India

[‡]Nanobiotechnology Laboratory, School of Biotechnology, Jawaharlal Nehru University, New Delhi 110067, India

*Corresponding author

[‖]These authors contributed equally to the manuscript.

Abstract

Hemoglobin A_0 (HbA_0) is a physiologically important tetrameric protein, consisting of two alpha (α) and two beta (β) subunits, resides inside the red blood cell and carries oxygen to the cell. In this study, the interaction of HbA_0 protein with anionic sodium dodecyl sulfate (SDS) has been investigated by small-angle neutron scattering (SANS), UV-visible spectroscopy, fluorescence spectroscopy, and circular dichroism (CD) spectroscopy. The previous studies on the HbA_0-surfactant system by DLS and spectroscopic techniques only confirmed the unfolding of HbA_0 without deciphering the exact process and differentiating between the subunit dissociation and extended structure formation. Our spectroscopic results reveal disruption of the heme pocket, loss of Tyr→Trp energy transfer, and spectral shifts indicative of methemoglobin formation. Utilizing the advantages of SANS, we have explored the subunit dissociation of tetramer units of HbA_0 and their different forms (monomer, dimer, etc.) with the sequential addition of SDS. The results reveal that the addition of SDS at low concentrations leads to the dissociation of tetramer structure into dimers and monomers, driven by molecular-level binding of SDS monomers to hydrophobic and electrostatic patches at the subunit interfaces rather than by micellization. Above higher SDS concentrations, a fraction of nonbound SDS forms free micelles that stabilize the dissociated monomers without promoting further unfolding. In the presence of electrolytes, electrostatic screening enhances protein–surfactant interactions and promotes the formation of extended rod-like complexes. These findings establish a detailed structural pathway for SDS-induced remodelling of HbA_0 and highlight the distinct behaviour of multimeric proteins compared to single-chain globular proteins.

Keywords: HbA_0, SDS, Spectroscopy, Subunit dissociation, SANS.

View Article Online
DOI: 10.1039/D6MA00049E

1. Introduction

Understanding different conformations of proteins is of principle importance as the unfolding/misfolding can cause different diseases e.g., Parkinson's, Alzheimer's, Cystic fibrosis, Cancer, etc. Surfactants are surface-active substance, that interacts strongly with protein due to their common amphiphilic nature, leading to an exhibition of rich phase behaviour in the aqueous solution [1,2]. The combination of protein with surfactants finds applications in pharmaceutical, cosmetic, food industries, etc. [3,4]. Therefore, the understanding of protein-surfactant interaction has an emerging scientific interest in terms of the conformational change of the protein.

Hemoglobin is one of the widely studied iron-containing proteins, which includes four polypeptide chains (a tetramer) consisting of a dimer of α-polypeptide and β-polypeptide chains ($a_2\beta_2$) and usually find in the red blood cells of many animals [5]. Each polypeptide chain is attached to a heme group, composed of a porphyrin ring and to which iron is attached. The heme group is the most active site in hemoglobin which can interact with different biologically active molecules [6]. Iron atoms in the hemoglobin bind reversibly with oxygen as blood travels between the lungs and the tissues. The oxygenated form (*R*-state) of hemoglobin is known as oxyhemoglobin which is bright red, whereas the reduced form or the deoxygenated form (*T*-state) of hemoglobin, known as methemoglobin, is brownish. The transformation between the *R* and *T*-state of hemoglobin is crucial for the transport of oxygen throughout the body [7]. Hemoglobin is a highly water-soluble protein and hence, demonstrates strong hydrophilic interactions with ionic surfactants [8–10]. The interactions between hemoglobin and surfactants play an important role in the field of biochemistry [11]. It is driven by both the electrostatic and hydrophobic interactions between the protein and surfactants [12–15]. Sodium dodecyl sulphate (SDS) is an anionic surfactant commonly used to study mechanisms of protein unfolding and various other structural changes [16]. Studies reveal that unlike other denaturants such as guanidinium hydrochloride and urea which denature proteins only at molar concentrations, SDS can denature proteins at millimolar concentrations [17–21]. SDS can perturb quaternary structure of Hemoglobin at very low concentrations (0-5mM), impacting activity, aggregation, and long-term stability. The efficiency of ionic surfactants as a denaturant can be tuned by adding salts, which are known to influence strongly the self-assembly of surfactants [22,23]. On the other hand, at low NaCl concentration (~0.2 M), hemoglobin exists mostly as tetramers, whereas at higher NaCl concentrations (≥1 M), it exists

View Article Online
DOI: 10.1039/D6MA00049E

predominantly as dimers. A molecular-level understanding of how SDS interacts with HbA_0 therefore provides valuable guidance for designing more stable protein-containing materials. Such insights are important for preventing unwanted subunit dissociation in Hemoglobin-based oxygen carriers, maintaining functional conformation in biosensors, and ensuring structural integrity in protein-loaded delivery systems. Mechanistic knowledge of surfactant-mediated destabilization helps inform formulation strategies, predict compatibility with material interfaces, and support rational engineering of protein material hybrids.

In this study, we investigate the interaction of HbA_0 with SDS across a broad range of surfactant concentrations using a combination of UV–visible spectroscopy, fluorescence spectroscopy, circular dichroism (CD), and small-angle neutron scattering (SANS). These complementary techniques enable a detailed analysis of both local changes in the heme environment and global alterations in secondary and quaternary structure. SANS allows us to distinguish tetramers, dimers, and monomers granularity not accessible through conventional spectroscopic approaches. We also examine the role of ionic strength, comparing protein–surfactant complexation in the presence and absence of electrolytes to assess electrostatic screening effects relevant to physiological and materials-processing conditions. All experiments were performed near the isoelectric point of HbA_0 [24], where the protein is most susceptible to structural perturbation.

Collectively, our results reveal the stepwise dissociation pathway of HbA_0 induced by SDS and demonstrate how surfactant concentration and ionic strength govern structural transitions. By bridging fundamental biophysical observations with materials-design implications, this work provides insight that is directly applicable to the development of stable protein-based formulations, nanocarriers, biosensors, and advanced biomaterials where surfactants are either intentionally incorporated or unavoidable during processing.

2. Materials and methods

2.1 Hemoglobin preparation

Hemoglobin A_0 (HbA_0; catalogue no.H0267) Sodium dodecyl sulphate (SDS; catalogue no. L4390) was purchased from Sigma-Aldrich. D_2O (99.9 atom % D) was used for the sample preparation to create the contrast for SANS experiments. For the rest of the experiments like UV-vis and CD, and fluorescence spectroscopy measurements H_2O was used. HbA_0 and SDS were dissolved in 20 mM phosphate buffer at pH=7.4. All HbA_o-SDS mixtures were incubated for an hour to equilibrate the solution at 25°C for optical spectroscopy measurements and

View Article Online
DOI: 10.1039/D6MA00049E

overnight at 30°C for SANS experiments, consistent with the respective instrument-controlled conditions.

2.2Small-Angle Neutron Scattering (SANS)

Small-angle neutron scattering experiments were carried out on the SANS-I diffractometer at the Guide Tube Laboratory, Dhruva Reactor, Bhabha Atomic Research Centre (BARC), India [25]. All the measurements were performed atλ=5.2 Å and the wavelength resolution ($\Delta\lambda/\lambda$) was ~15%. All the Samples were placed in 5 mm HELLMA quartz cuvettes and aligned t the neutron beam inside the thermostatic sample holder maintained at 30 °C. The detection of the scattered neutrons was performed using a one-dimensional detector in the q-range of 0.017 to 0.35 $Å^{-1}$. The background, empty cell contributions, and transmission corrections were performed on the raw data and normalized to the absolute cross-sectional unit using standard protocols. Finally the data obtained from SANS experiments were fitted using the analysis software named SASfit[26].

The differential scattering cross-section per unit volume ($d\Sigma/d\Omega$) as a function of q for monodisperse interacting particles is given by

$$\left(\frac{d\Sigma}{d\Omega}\right)(q) = N_p P(q) S(q) + B \tag{1}$$

where N_p, $P(q)$, and $S(q)$ are the number density of particle, form factor and structure factor, respectively, and B is the incoherent background that arises due to the hydrogen present in different components. The form factor of HbA_0 protein and SDS micelles has been assumed to be prolate ellipsoidal with axial anisotropy ε[21,27]. For the semi-axes R, R and εR, $P(q)$ can be written as

$$P(q) = \langle F^2(q) \rangle = \int_0^{\pi/2} \left[F\left(q, R_1\right) \right]^2 \sin\beta \, d\beta \tag{2}$$

where $F\left(q, R_1\right) = \left(\rho_p - \rho_s\right) V \left\{ \frac{3J_1\left(qR_1\right)}{qR_1} \right\}$

with $J_1(x) = \frac{(\sin x - x\cos x)}{x^2}$, $R_1 = R\left(\sin^2\beta + \varepsilon^2 \cos^2\beta\right)^{1/2}$

where $\rho_p$and ρ_s are respectively the scattering length densities of the particle and solvent. V is the volume of the particle, β is the angle between the directions of the semimajor axis and wave vector transfer, and $J_1(x)$ is a first-order spherical Bessel function.

View Article Online
DOI: 10.1039/D0MA00049E

The wormlike micellar model has been used to define the elongated structure of the complex [28]. In this model, the total length (contour length) can be described by a chain with number of locally stiff statistical segments. This segment, *l*p (persistence length), is the length of the cylinder over which the flexible cylinder can be considered as a rigid rod. In wormlike micellar model, the Kuhn length (*b*), describes the stiffness of a chain and is related to the persistence of length by *b*=2*l*p.The structure factor of charged particles interacting through the screened Coulomb potential is used to define the scattering profile of pure ionic surfactants. The charged particles are assumed to be rigid spheres of equivalent size σ interacting through a potential as given by[27]

$$u(r) = u_0\sigma \frac{\exp\left[-\kappa(r-\sigma)\right]}{r}, r\rangle\sigma \quad (3)$$

where κ is the Debye- Hückel inverse screening length and u_0 is the contact potential**,** r is Inter particle distance and σ is the hard sphere diameter of particles respectively.

.

A two-step approach has been adapted to analyze the SANS results qualitatively and quantitatively. In the first step, an Indirect Fourier Transformation (IFT) has been performed using Sasview software (http://www.sasview.org) to obtain the model-independent information of the scattering objects in the real space [29]. The IFT of scattering data provides the pair distance distribution function ($p(r)$). The information about the maximum size D_{max} ($p(r)$~0 at $r=D_{max}$) and the radius of gyration (R_g) of the scattering objects are obtained from $p(r)$. In the second step, a detailed model for HbA_0-SDS complexes has been proposed based on the information obtained from the $p(r)$ and optimizing the nonlinear least-squares fitting method.

2.3 UV-visible spectroscopy

For the protein-surfactant interaction study, the reaction between HbA_0 at a working concentration of 0.1 mg/mL and different concentrations of SDS was set up and incubated for an hour. A wavelength scan has been performed from 200 nm to 700 nm using the PerkinElmer Lambda-365 UV-vis spectrophotometer. The absorbance as a function of wavelength has been extracted and plotted using GraphPad Prism 9.

2.4 Fluorescence spectroscopy

View Article Online
DOI: 10.1039/D6MA00049E

Similar to UV-vis spectroscopic study, the concentration of HbA_0 was kept constant at 0.1 mg/mL while the concentration of SDS was varied and incubated for an hour. The emission (Em) scan at different excitation (Ex) wavelengths (273 nm and 295 nm, respectively with slit width 5 nm) was performed using the Cary eclipse fluorescence spectrometer. The measurements yield the intensity as a function of wavelength, which has been plotted using GraphPad Prism 9.

2.5 Circular Dichroism (CD) spectroscopy

CD measurements were carried out with a Jasco J-600 spectrophotometer equipped with a Peltier temperature controller. The sample temperature was fixed at 25 ^{0}C with a thermostatically controlled cell holder throughout the measurement. Secondary structure was measured over the wavelength of 190 to 250 nm using a 1 mm HELLMA quartz cuvette. CD spectra were collected with a fixed scan speed of 10 nm min^{-1} and each spectrum was averaged over three scans. The high-tension voltage for the spectra was restricted to be less than 600 V. This condition was achieved keeping the HbA_0 concentration as low as 0.1 mg/mL. All the protein-surfactant complexes were stabilized for an hour before performing the measurements. The results are expressed in terms of mean residue ellipticity (MRE) expressed in units of degcm^{2}dmol^{-1}. The MRE can be defined as

$$MRE = \frac{\theta_{obs}}{nlC} \tag{4}$$

where θ_{obs} is the CD in millidegree, n is the number of amino acid residues, l is the path length of the cuvette in cm and C is the concentration of the protein in molL^{-1}.

2.6 Bright-Field Microscopy

Bright-field microscopy was used to qualitatively assess the morphological appearance of Hemoglobin (HbA_0) in the presence of increasing concentrations of sodium dodecyl sulfate (SDS). HbA_0 solutions were prepared at the same concentration used for spectroscopic and SANS measurements and incubated with SDS at specified concentrations (0.01–10 mM) in Tris buffer (pH 7.4). All samples were equilibrated at room temperature for a fixed duration prior to imaging.

For imaging, a small aliquot of each sample was placed onto a clean glass microscope slide and covered with a coverslip. Bright-field images were acquired using an optical microscope equipped with a 10× objective lens and a 10× eyepiece (total magnification 100×) under white-

View Article Online
DOI: 10.1039/D6MA00049E

light illumination. All images were collected using identical magnification, illumination, and exposure settings to allow qualitative comparison across different SDS concentrations. No staining or fixation was applied to avoid perturbation of the native solution-phase assemblies. The images were used solely for qualitative visualization of macroscopic aggregation and heterogeneity.

2.7 Dynamic Light Scattering (DLS)

Dynamic light scattering (DLS) measurements were performed using Malvern Zetasizer Nano series (ZEN3600) to determine the hydrodynamic size of Hemoglobin A_0 (HbA_0) in the presence of sodium dodecyl sulfate (SDS) and varying ionic strength. All measurements were carried out using a Malvern Zetasizer Nano series instrument equipped with a 633 nm He–Ne laser and a backscattering detection angle of 173°. HbA_0 was prepared at a concentration of 0.1 mg/mL in 20 mM phosphate buffer (pH 7.4). SDS solutions of varying concentrations (0–80 mM) were prepared in the same buffer and mixed with HbA_0 to obtain the desired protein–surfactant systems. For ionic strength studies, NaCl was added to HbA_0 solutions containing 40 mM SDS to achieve concentrations ranging from 0 to 0.8 M. All samples were incubated for 1 hour at room temperature (25 °C) to ensure equilibration prior to measurements. The solutions were filtered through a 0.22 μm syringe filter to remove dust and large particulates before analysis. DLS measurements were conducted at 25 °C, and each sample was measured in triplicate with an equilibration time of 120 seconds per run. The hydrodynamic diameter was calculated using the cumulant analysis method provided by the instrument software. The reported values represent the mean hydrodynamic size ± standard deviation (SD) of three independent measurements.

3. Results

3.1 Study of HbA_0-SDS interaction

3.1.1 UV-visible spectroscopic study of HbA_0 and SDS interaction:

UV-visible spectroscopy has been performed to determine the structural transition of HbA_0 in the backbone of the protein. The interaction of HbA_0 with SDS has been carried out for the surfactant concentration range of 0 to 40 mM. HbA_0 shows a strong absorbance at 414nm, which denotes the oxy HbA_0 and the presence of the Fe^{2+} facilitating the binding of oxygen through the coordinate covalent bond. The double peak at 540 nm and 575 nm also

View Article Online
DOI: 10.1039/D6MA00049E

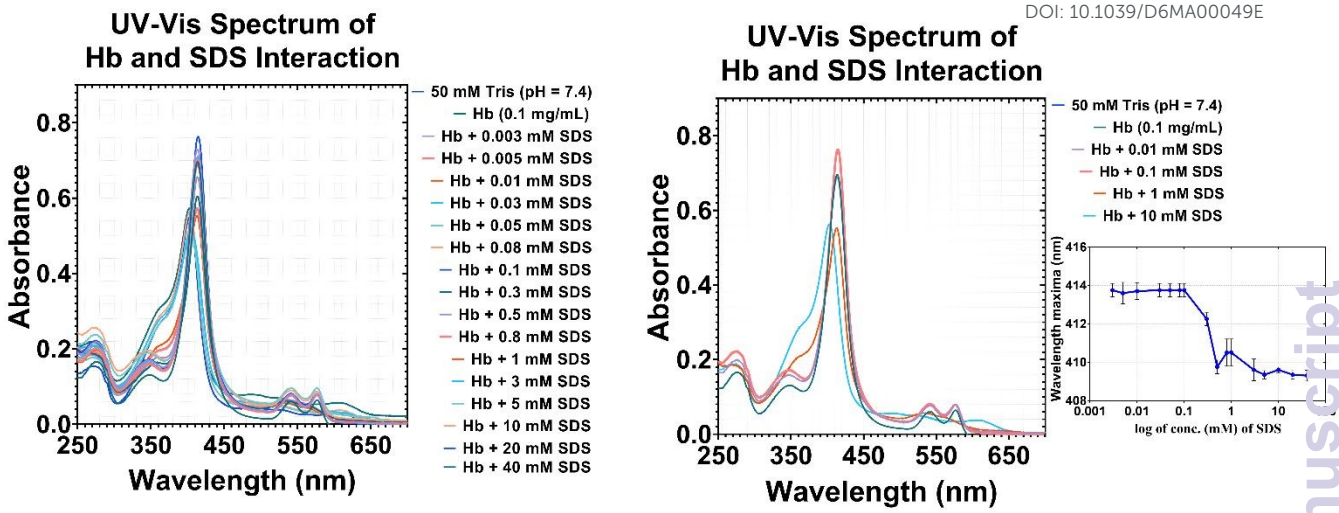

Figure 1: Absorbance spectra of HbA_0 (0.1 mg/mL) interaction with SDS (0.003 mM - 40 mM). 50 mM Tris buffer (pH = 7.4) used as reference. All the spectra shown here are normalized with their SDS only spectra respectively. The inset graph represents the shift in the wavelength maxima of HbA_0 from 414 nm – 408 nm during unfolding.

signifies the oxy HbA_0 form. The release of oxygen converts oxyhemoglobin into its deoxygenated form, which is signified by the disappearance of the characteristic bands at 540 nm and 575 nm. This transition occurs because SDS perturbs the heme pocket by disrupting the hydrophobic and electrostatic interactions that stabilize the Fe^{2+}–O_2 coordination. The destabilization weakens the ligand environment surrounding the heme group, making the iron center more susceptible to oxidation. As a result, Fe^{2+} is readily oxidized to Fe^{3+}, forming methemoglobin. This oxidation process not only abolishes oxygen binding but also leads to the observed shift of the Soret peak from 414 nm to approximately 408 nm, accompanied by an increased absorbance near 395 nm corresponding to free heme. Together, these changes indicate SDS-induced destabilization of the heme environment, oxygen release, and subsequent formation of methemoglobin[30]. The UV-Vis absorbance spectrum of pristine HbA_0 has been compared with the UV-Vis absorbance spectra of the HbA_0 in presence of different concentrations of SDS. The results indicate that at very low concentrations of SDS (0.003 mM to 0.3 mM), there is no significant change in the HbA_0 spectra. However, at higher SDS concentrations (3 mM to 40 mM), HbA_0 soret peak (at 414 nm) and shift towards 408 nm with the formation of methemoglobin. The disappearance of the oxyhemoglobin peak (540 nm and 575 nm) supports the formation of methemoglobin. The shift is also accompanied by the heme loss, which can be visualized by the increase in the 395 nm absorbance peak associated with the free heme group (Figure 1). These findings correlate to the fact that SDS binds to the HbA_0

View Article Online
DOI: 10.1039/D6MA00049E

and imparts structural changes. It also binds and destabilizes the heme group binding pocket which is localized in the hydrophobic domains of hemoglobin and is the site of oxygen binding [31,32].

3.1.2 Fluorescence spectroscopic study of HbA_0 and SDS interaction:

The changes in the structural conformation of HbA_0 in presence of 0 to 40 mM SDS have also been confirmed by the Fluorescence spectroscopy. The amino acids tyrosine (Ex-273 nm and Em-305 nm) and tryptophan (Ex-295 nm and Em-335 nm) have intrinsic fluorescence, which has been utilized to study the protein conformation [33,34]. Excitation of HbA_0 at 273 nm gives the emission maximum at 335 nm, signifies the Fluorescence Resonance Energy Transfer (FRET) between the tyrosine and the tryptophan as the emission of tyrosine nearly matches with the excitation of the tryptophan. Figure 2(A) shows that there is no change in the emission maxima of HbA_0 up to 0.1 mM concentration of SDS. A gradual increase in the fluorescence intensity at the SDS concentration of 0.3 mM has been observed due to the unfolding of HbA_0. The increase in fluorescence intensity has also accompanied by the gradual shift in the emission maxima towards 305 nm which indicates the hindering of the FRET process between tyrosine and tryptophan due to the disruption in the native HbA_0 structure. This process continues till the SDS concentration of 5 mM and finally it is stabilized at 10 mM. This also supports the gradual changes obtained from the SANS experiments and may be due to the subunit dissociation. Figure 2(B) shows the Fluorescence emission of HbA_0 when excited at 295 nm. The emission spectra observed is only due to the tryptophan residues without showing significant presence of FRET. The emission maximum has been found at 335 nm. A similar increase in the fluorescence intensity has been observed above the concentration of 0.3 mM SDS. The changes are directly correlated with the spectra obtained from the HbA_0 excitation at 275 nm except the FRET. The peak is started shifting towards the lower wavelength from the SDS concentration of 0.3 mM. The emission peak is started increasing significantly from this concentration till 1.0 mM and takes a sudden jump as seen from the increase in the peak height at SDS concentrations 3 mM and 5 mM. The emission spectra show minor increase in peak height at 10 mM SDS and above while exiting at 275 nm.

View Article Online
DOI: 10.1039/D6MA00049E

(A)

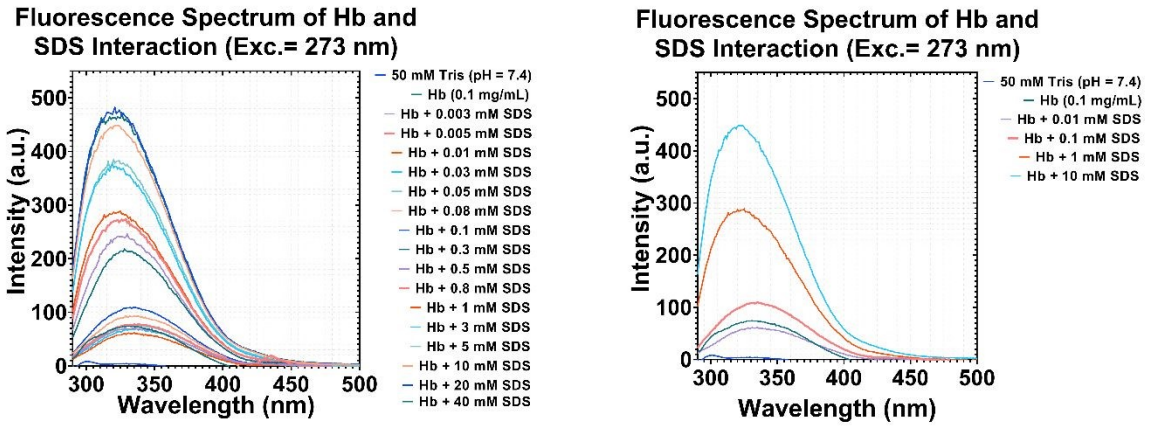

(B)

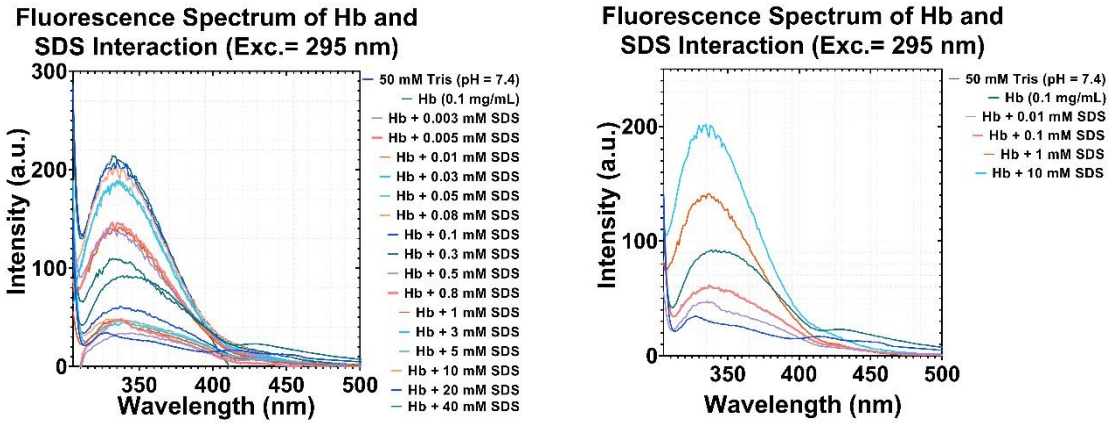

Figure 2: (A) Emission spectra (excitation= 273 nm) of Hemoglobin (0.1 mg/mL) interaction with SDS (0.003 mM - 40 mM). 50 mM Tris buffer (pH = 7.4) used as reference. All the spectra shown here are normalized with their SDS only spectra respectively and **(B)** Emission spectra (excitation = 295 nm) of Hemoglobin (0.1 mg/mL) interaction with SDS (0.003 mM - 40 mM.50 mM Tris buffer (pH = 7.4) used as reference. All the spectra shown here are normalized with their SDS only spectra respectively.

3.1.3 CD Spectroscopy to study the secondary structure alterations during HbA_0 and SDS interaction:

The conformational changes in HbA_0 due to the interaction with SDS was evaluated using CD Spectroscopy. The study shows two characteristics minima of α-helix structure at 208 nm and 222 nm (Figure 3). The addition of SDS in the concentration range of 0.01 mM to 0.1 mM gradually reduces the α-helix content of the HbA_0 protein. The decrease in α-helix content is compensated by the gradual increase in theβ-sheet structure. Above 0.1 mM the gain in the α-

helix content has been observed until it achieves the α-helix content of pristine HbA$_0$ at 1.0 mM and thereafter become constant. The β-sheet content follows the reverse trend compared to the α-helix one but also achieve the stability above 1.0 mM SDS concentration.

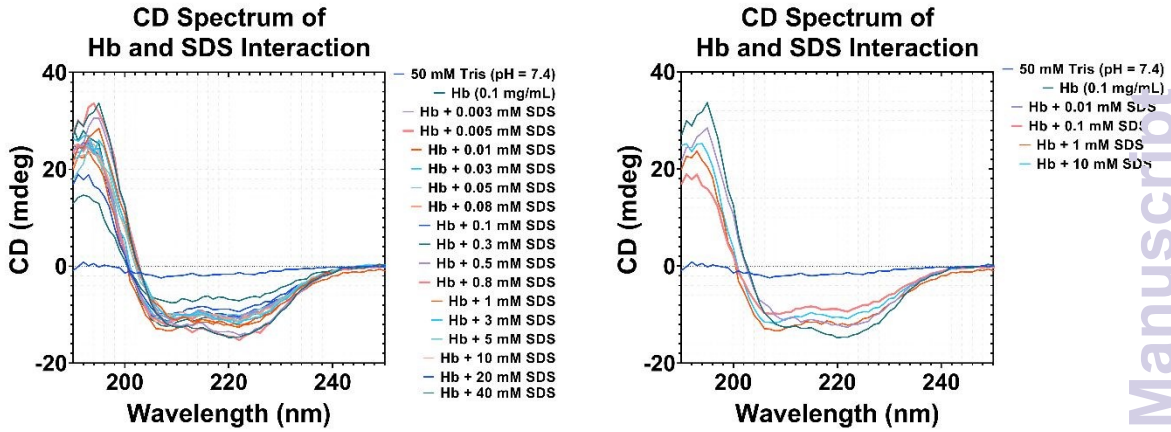

Figure 3: Far UV CD spectra of Hemoglobin (0.1 mg/mL) interaction with SDS (0.001 mM - 40 mM. 50 mM Tris buffer (pH = 7.4) used as reference.

Table 1: Percentage of Secondary structures (Predicted using K2D3) of Hemoglobin (0.1 mg/mL) interaction with SDS (0.001 mM - 40 mM. 50 mM Tris Buffer (pH = 7.4) used as reference.

Hb+SDS (mM)	% Alpha	% Beta
0	67.12±2.51	9.85±0.05
0.001	67.12±2.33	9.85±0.06
0.008	67.12±1.57	9.85±0.03
0.05	67.12±2.74	9.85±0.15
0.08	46.02±1.42	11.72±0.96
0.1	46.35±1.34	11.64±0.94
0.5	61.34±2.16	10.03±0.06
0.8	63.12±1.46	9.98±0.05

View Article Online
DOI: 10.1039/D6MA00049E

1	63.12±1.52	9.98±0.03
5	61.34±1.95	10.03±0.04
20	63.12±2.31	9.98±0.07
40	66.5±2.66	9.87±0.07

3.2 Characterization of HbA_0 SDS interaction using SANS

3.2.1 Characterization of pure HbA_0 and SDS in presence and absence of salt

The SANS data from individual components of 1 wt % HbA_0 protein and 40 mM SDS are shown in Figure 4. The scattering profile of 1wt% HbA_0 indicates the absence of interparticle interaction ($S(q)\sim1$) and therefore has been fitted by the form factor contribution alone. The obtained SANS scattering intensities are compared first to those calculated from the crystal data of HbA_0 on the Protein Data Bank (1GZX) using CRYSON software [35,36]. The calculated intensity from the crystal structure evidencing that the measured HbA_0 protein is correctly folded in the phosphate buffer. The analysis with the spherical form factor provides a radius of 28.3±0.7 Å, which is in good agreement with published results [37,38]. However, the IFT of SANS shows an axial anisotropy (Figure 4) and hence the data has been also fitted by prolate ellipsoidal form factor, which provides a better fitting, optimizing the reduced χ^2value. Interestingly, the effective size obtained from ellipsoid fitting is quite close to the fitted radius by the spherical object. Also, the radius of gyration (R_g) obtained from the model fitting (R_g=23.1 Å) is reasonably close to the R_g obtained from the Guinier approximation in the low-q regime [34].

In the case of SDS micelles, unlike HbA_0, SANS data cannot be fitted by $P(q)$ only and hence the contribution from $S(q)$ needs to be included. The higher number density of SDS micelles as compared to that of the 1 wt% HbA_0 protein in the respective systems could be the reason of arising the interparticle interaction in the system. The data of SDS micelles are fitted with the $S(q)$ of charged particles interacting through screened Coulomb interaction as mentioned in eq. 3 [39]. Specifically, Hayter-Penfold (HP) potential has been used to calculate the structure factor contribution of SDS micelles [40]. It has been observed that the size of SDS micelles increases, whereas the effective charge decreases with an increase in salt concentration. The structural parameters of the SDS micelles as obtained from SANS fitting

View Article Online
DOI: 10.1039/D0MA00049E

are in good agreement with the literature [41]. The fitted parameters of the HbA_0 protein and SDS micelles at different salt concentrations are given in Table 2.

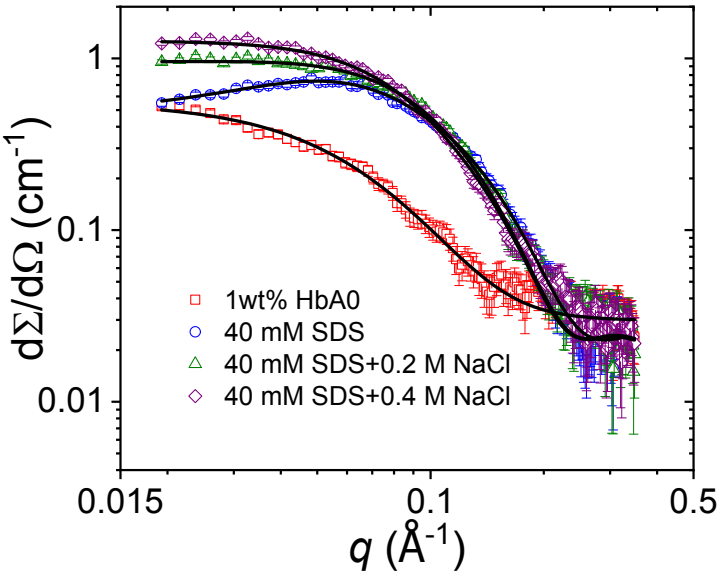

Figure 4:SANS data of 1 wt % HbA_0 protein and 40 mM of anionic SDS at pH = 7.4 and 0, 0.2, and 0.4 M NaCl in D_2O.

Table 2: The fitted structural parameters of SANS data of individual components of HbA_0 protein and SDS surfactant at pH = 7.4 and 0, 0.2, 0.4 M NaCl in D_2O. The aggregation number of micelles is calculated by dividing the micellar volume by the volume of the surfactant molecule.

System	Shape	Semi-major axis εR (Å)	Semi-minor axis R (Å)	Axial Anisotropy (ε)	Effective radius (Å)	Charge (e.u.)
1 wt% HbA_0	Prolate ellipsoid	64.6	18.8	3.44	28.3±0.7	-
40 mM SDS	Prolate ellipsoid	27.8	16.7	1.43	18.8±0.5	-25.2
40 mM SDS+0.2 M NaCl	Prolate ellipsoid	32.3	16.7	1.93	20.8±0.5	-23.4

View Article Online
DOI: 10.1039/D6MA00049E

40 mM SDS+0.4 M NaCl	Prolate ellipsoid	41.6	16.7	2.49	22.6±0.6	-19.0

3.2.2 Effect of surfactant (SDS) concentration on HbA_0 unfolding

SANS measurement has been carried out for 1wt% HbA_0 protein with varying concentrations of SDS (0-80 mM). SANS results with model fitting are shown in Figure 5(A), whereas the IFT of these data is presented in Figure 5(B). The IFT of 1wt% HbA_0 shows the appearance of a broad maximum around r=30 Å**,** which is in agreement with the resultobtainedfrom the model fitting of SANS data. The maximum of the $p(r)$ function shifts towards the lower-r on the addition of SDS in the protein solution. The maximum, which appears at 23.9Å for 1wt% HbA_0 with 5 mM SDS, shifts to 21.2 Å at 10 mM SDS and 19.2 Å at 20 mM SDS concentrations and thereafter becomes constant. Following the similar trend, the maximum dimension of the complex (D_{max}) also decreases with the addition of SDS. D_{max}, which is obtained ~90 Å for pristine HbA_0 protein, decreases to as low as ~42 Å in presence of 80 mM SDS. Another interesting feature obtained from $p(r)$ is that with an increase in the SDS concentration, the amplitude of oscillation also increases, which indicates the occurrence of a better-defined micelle structure or an increase in the number of micelles.

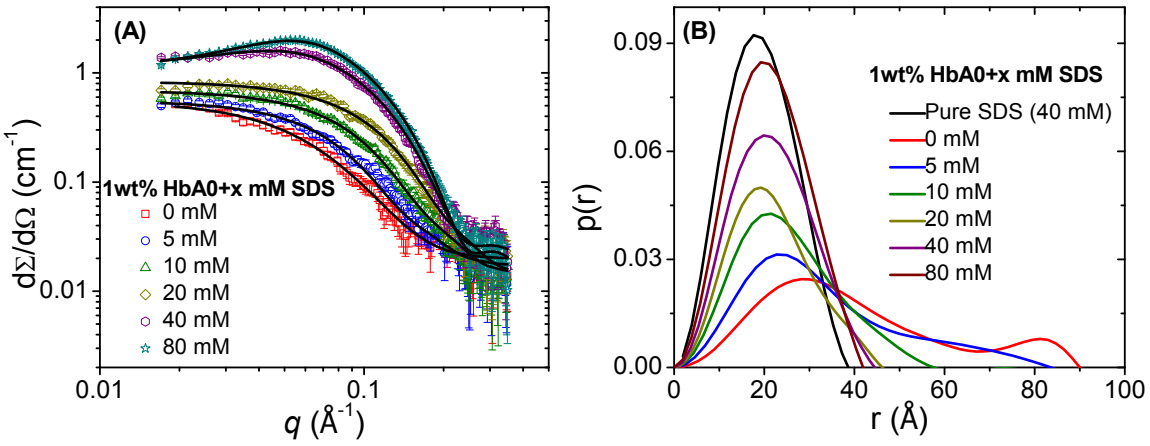

Figure 5: (A) SANS profiles of 1 wt% HbA_0 in the presence of 0-80 mM SDS. (B) Pair-distance distribution functions $p(r)$ obtained from the fits of the experimental data. The black continuous lines indicate the model fitting of SANS results.

The mismatch between the sum of the scattering contribution of the individual protein and surfactant with the scattering of protein-surfactant complexes rules out the non-interacting behavior of HbA_0 and SDS. The interaction between HbA_0 and SDS has been accounted for

View Article Online
DOI: 10.1039/D0MA00049E

by the ellipsoidal shape form factor, chosen based on the $p(r)$ analysis of the SANS data. The analysis shows that the effective size of the protein-surfactant complexes decreases from 29.6 Å to 24.3 Å on the addition of 5 mM SDS and further decreases to ~19.5 Å at 20 mM SDS and thereafter becomes almost constant. The result implies that at lower SDS concentration (5 mM), the electrostatic interaction of surfactant with HbA_0 protein allows the dissociation of most of the tetramer units into dimer and or monomer units while a part of HbA_0 protein remains intact as tetramers. An attempt has been taken to quantify the number of dissociated subunits of HbA_0 protein in each step of SDS addition from the absolute scaling of SANS data. However, the quantification is not as straightforward as for other globular proteins like Bovine Serum Albumin (BSA). In the case of BSA, the ionic surfactants form micelles along the randomly distributed unfolded polypeptide chain of the protein [21,42,43]. The formation of beads-on-a-string-like complexes as a result of protein unfolding can be seen from the change in the functionality of the scattering data. On the contrary, in tetrameric proteins like HbA_0, the ionic surfactant only dissociates their subunits rather than opening up the polymeric chain. Moreover, the hydrogen-deuterium (H/D) exchange makes it more complicated in determining the exact contrast between HbA_0 and solvent. A study shows that up to 950 hydrogen atoms can be exchanged with deuterium while dissolving HbA_0 in D_2O and equilibrate for a long time [37]. In order to ensure the maximum H/D exchange, all the measured sample for SANS were equilibrated overnight. The estimated number densities of the scattering objects obtained from the scaling using eq. 1 are shown in Table 3. The analysis shows that the number of subunits goes up to ~2 times and □5 times compared to the pristine HbA_0 on the addition of 5 and 10 mM SDS, respectively. This trend continues till 20 mM SDS and thereafter becomes constant. However, the propensity of increase in the number density significantly decreases above 10 mM SDS concentration. At the end of subunit dissociation, the number density of HbA_0 in protein-surfactant complexes increases □6 times compared to the pristine protein. It should be mentioned here that one tetramer unit dissociates to either two dimers or four monomers' subunits. Therefore, the number is somehow an overestimation, which may be due to the approximation taken for H/D exchange in the protein. The typical scattering length density of hemoglobin is ~2.0×10^{10} cm^{-2} in H_2O solvent but can increase to ~3.0×10^{10} cm^{-2} in D_2O at full H/D exchange, depending on the specific protein concentration, and exact level of H/D exchange. In our case, we have incubated all the samples for overnight to allow the exchange of H/D in the protein. However, this incubation time may not be sufficient for full H/D exchange. Therefore, assuming complete exchange of H/D in the protein for analysis leads to

error up to ~60% in the number density of the dissociated subunits and may caused the overestimation in the number density.

Table 3: Fitted parameters of SANS data of protein-surfactant systems (1 wt% HbA_0 + c_i mM SDS).

System	Structure	SDS (mM)	D_{max} (Å)	Semi-minor Axis R (Å)	Axial Anisotropy (ε)	R_{eff} (Å)[e]	Free micelle concentration (mM)	Estimated Number density of subunits
1wt% HbA_0+ c_i mM SDS	Ellipsoid	0	90	18.8	3.44	28.3±0.8	0	2.5×10^{17}
		5	83	16.7	3.04	24.2±0.7	0	4.8×10^{17}
		10	57	16.7	2.11	21.4±0.6	0	1.2×10^{18}
		20	46	16.7	1.76	20.2±0.5	8	1.6×10^{18}
		40	45	16.7	1.80	20.3±0.6	15	1.7×10^{18}
		80	42	16.7	1.79	20.3±0.5	45	1.6×10^{18}

The subunit dissociation of HbA_0 with SDS has also been explained in terms of change in the size of the scattering objects as the size of the tetramer (R_T) is related to the size of the dimer (R_D) and monomer (R_M) by $R_T=2^{1/3}\,R_D$ and $R_T=2^{2/3}\,R_M$, respectively [44]. The effective size of 1wt% HbA_0-5 mM SDS complexes is obtained as 24.3 Å, thus suggesting that most of the tetramer units of the HbA_0 protein are dissociated into dimer or monomer form. The dissociation of tetramers continues with the further addition of SDS (10 mM) and as a consequence, the decrease in the size of the complexes has been observed. The size of 1wt% HbA_0-10 mM SDS complexes has been obtained as 21.4 Å, which implies the further dissociation of dimer unit into monomer form. The increase in the number density also supports further dissociation of HbA_0 (Table 3). The further increase in the SDS concentration (20 mM) dissociates most of the tetramer and dimer units to monomer and thereafter, the dissociation of HbA_0 stops as reflected from the constant effective size of the complexes at higher SDS concentrations (≥20 mM). This is why the positions of the maximum in the $p(r)$ function remain the same for 1wt% HbA_0 with 20-80 mM SDS. The excess of surfactants that are not bound to the protein coexists as micelles with the protein-surfactant complexes and contributes to the increase in the scattering intensity at low-q and amplitude of the maximum in $p(r)$ function.

View Article Online
DOI: 10.1039/D0MA00049E

The excess surfactant micelles are fitted by the prolate ellipsoid form factor combined with the Hayter-Penfold potential [45]. The fitted parameters of the protein-surfactant complexes are given in Table 3.

3.2.2 Effect of ionic strength on SDS mediated HbA_0 unfolding

The effect of ionic strength on HbA_0-SDS interaction and subsequent complex formation have also been studied. SANS measurements have been carried out for 1wt% HbA_0-40 mM SDS complexes with different concentrations of NaCl (0 to 0.8 M) (Figure 6). Under these solution conditions, the pristine HbA_0 protein are expected to be in the form of tetramers [46]. The model fitting of SANS results is shown in Figure 6(A), whereas the IFT of these data are presented in Figure 6(B). The scattering of pristine HbA_0 in presence of salt could not be measured due the strong electrostatic attraction, leading to the aggregation and hence phase separation from the solution. On the contrary, the presence of 40 mM SDS is able stabilized HbA_0 in the electrolyte solution. In order to account the simultaneous changes in the both of these structures (HbA_0-SDS complexes and free SDS micelles), the SANS measurements also been performed for pure SDS micelles at different NaCl concentrations (0, 0.2, and 0.4 M) (Figure 4). The analysis of the $p(r)$ function shows that the position of the maximum marginally shifts while the maximum dimension (D_{max}) significantly shifts towards higher-r with an increase in the salt concentration. The marginal shift of the maximum of $p(r)$ can be accounted for by the increase in the size of SDS micelles but could not explain the extended $D_{max}$of the complex. On the other hand, the assumption of extended form of the HbA_0-SDS complexes could explain the significant increase in D_{max} at higher salt concentrations.

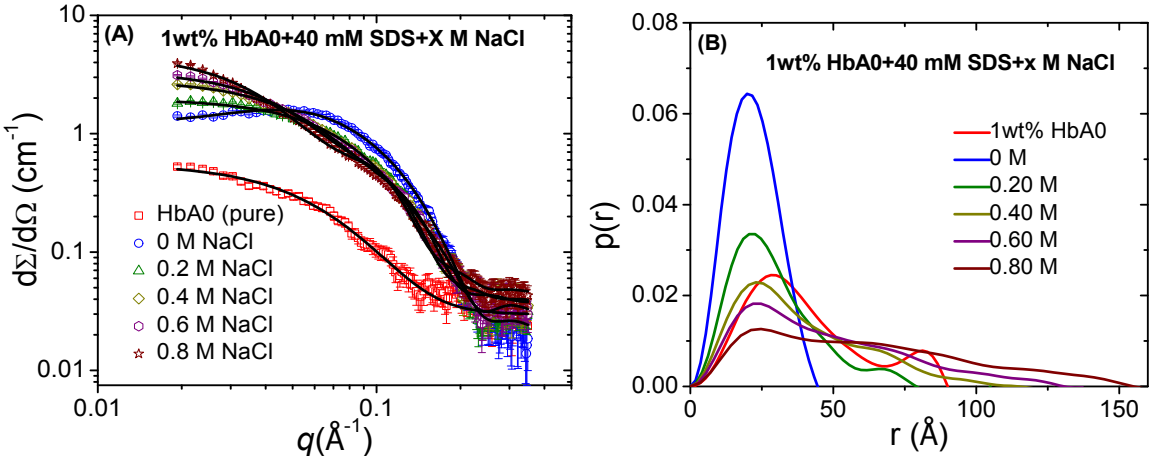

Figure 6:(A) SANS profiles of 1 wt% Hb with 40 mM SDS for varying salt concentration from 0 to 0.8 M NaCl and **(B)** Pair distance distribution functions $p(r)$ obtained from the fits of the experimental data.

View Article Online
DOI: 10.1039/D0MA00049E

Table 4: Fitted parameters of SANS data of protein-surfactant systems (1 wt% HbA_o + 40 mM SDS + c_s M NaCl).

System	Structure	NaCl (M)	D_{max}(Å)	Semi-major axis εR (Å)	Semi-minor axis R (Å)	Axial Anisotropy (ε)	Effective radius (Å)
1wt% HbA_0+40 mM SDS	Ellipsoid	0	45	29.9	16.7	1.79	20.3
		0.2	79	57.7	17.7	3.26	26.2
		0.4	112	79.8	18.1	4.40	29.7
		0.6	112	92.7	17.4	5.33	30.4
	Worm-like micelles	0.8	Cross-section radius = 15.5 Å, Kuhn length = 118.0 Å Contour length = 262.5 Å				

The SANS spectra at high and mid-q regimes are close to each other, suggesting that there is only a marginal change in the smaller dimension of the HbA_0-SDS complexes at different NaCl concentrations.In the low-q regime, the scattering intensity increases at higher salt concentrations, supporting the formation of bigger HbA_0-SDS complexes. The analysis of SANS data shows that HbA_0-SDS complexes of prolate ellipsoidal structure with the semi-minor axis of 16.7 Å are formed. The increase in the salt concentration increases the axial anisotropy (ε) and leading to the formation of worm-like micelle in presence of 0.8 M NaCl. The cross-section radius, Kuhn length, and contour length are 15.5 Å, 118.0 Å, and 262.5 Å, respectively. Thus, the results suggest that the addition of salt makes HbA_o protein more interactive with SDS surfactant.

3.3 Bright-Field Microscopy Analysis

Bright-field microscopy was employed to examine the morphological appearance of hemoglobin (HbA_0) in the presence of increasing concentrations of SDS. Representative images of Tris buffer and HbA_0 alone show a uniformly dispersed appearance with no visible large-scale aggregates. At low SDS concentrations (0.01-0.1 mM), the samples remain

View Article Online
DOI: 10.1039/D6MA00049E

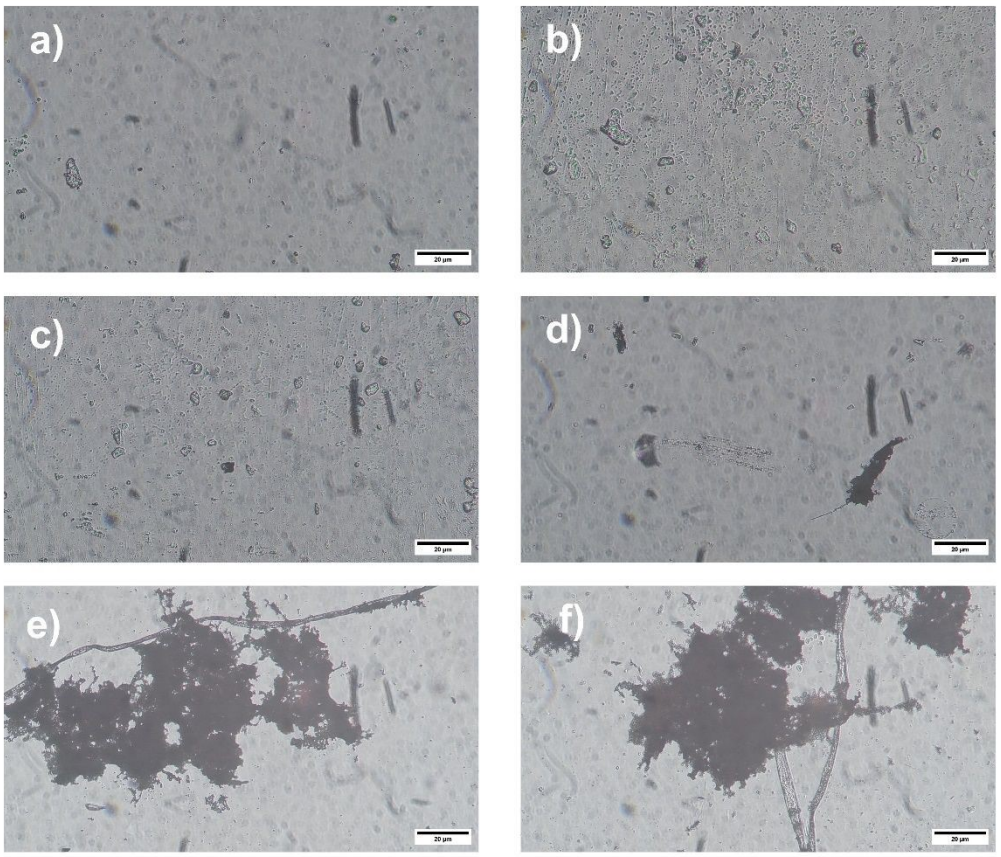

Figure 7: Bright-field microscopy images of Hemoglobin (HbA_0) in the presence of increasing SDS concentrations. Representative bright-field images of (a) Tris buffer only, (b) HbA_0 only, (c) HbA_0 + 0.01 mM SDS, (d) HbA_0 + 0.1 mM SDS, (e) HbA_0 + 1 mM SDS, and (f) HbA_0 + 10 mM SDS are shown. At low SDS concentrations (≤0.1 mM), the samples appear optically homogeneous with no visible large-scale aggregates. At higher SDS concentrations (≥1 mM), dark, irregular features become apparent, indicating increased heterogeneity and the formation of larger protein–surfactant assemblies. All images were acquired under identical imaging conditions using a 10× objective and 10× eyepiece (total magnification 100×). No staining or fixation was applied.

optically homogeneous and comparable to pristine HbA_0, indicating the absence of detectable macroscopic aggregation. Upon increasing the SDS concentration to 1 mM, the appearance of dark, irregular features becomes evident, suggesting the formation of larger protein–surfactant assemblies. At the highest SDS concentration examined (10 mM), these features become more pronounced and widespread, reflecting increased heterogeneity and aggregation within the

View Article Online
DOI:10.1039/D5MA00049E

sample. All images were acquired under identical imaging conditions to allow qualitative comparison across concentrations.

3.4 Dynamic Light Scattering (DLS) Analysis of HbA_0-SDS Interaction

To complement the structural insights obtained from SANS and spectroscopic techniques, dynamic light scattering (DLS) measurements were performed to probe the hydrodynamic size evolution of HbA_0 in the presence of SDS and varying ionic strength. The results are summarized in Figure 8. In the absence of SDS, HbA_0 exhibited a hydrodynamic diameter of 6.5 ± 0.3 nm, consistent with its native tetrameric state in solution [47]. Upon gradual addition of SDS (0-20 mM), a systematic decrease in hydrodynamic size was observed, reaching ~4.3 ± 0.3 nm at 20 mM SDS, followed by a plateau at higher concentrations (40-80 mM). This reduction in hydrodynamic dimension indicates progressive dissociation of tetrameric HbA_0 into smaller subunits and the formation of stabilized protein–surfactant complexes, in agreement with SANS-derived structural parameters. The effect of ionic strength was further examined for HbA_0 in the presence of 40 mM SDS. A pronounced increase in hydrodynamic size was observed with increasing NaCl concentration, from ~4.3 ± 0.2 nm (0 M) to ~63.5 ± 5.4 nm (0.8 M NaCl). The significantly larger size of HbA_0–SDS complexes relative to SDS micelles indicates enhanced protein–surfactant association and confirm the formation of worm-like structure.

All DLS measurements were conducted at 0.05 mg/mL, since higher concentrations (e.g., 10 mg/mL used in SANS) are unreliable due to multiple scattering and apparent aggregation that bias size distributions. Despite this, DLS trends remain directly comparable to SANS, as both capture the same structural transitions. Absolute DLS sizes are larger than dry dimensions due to hydration and diffusive effects. Overall, DLS independently validates SANS, confirming (i) SDS-induced HbA_0 dissociation at low surfactant concentrations and (ii) formation of larger, salt-induced assemblies at higher ionic strength.

View Article Online
DOI: 10.1039/D6MA00049E

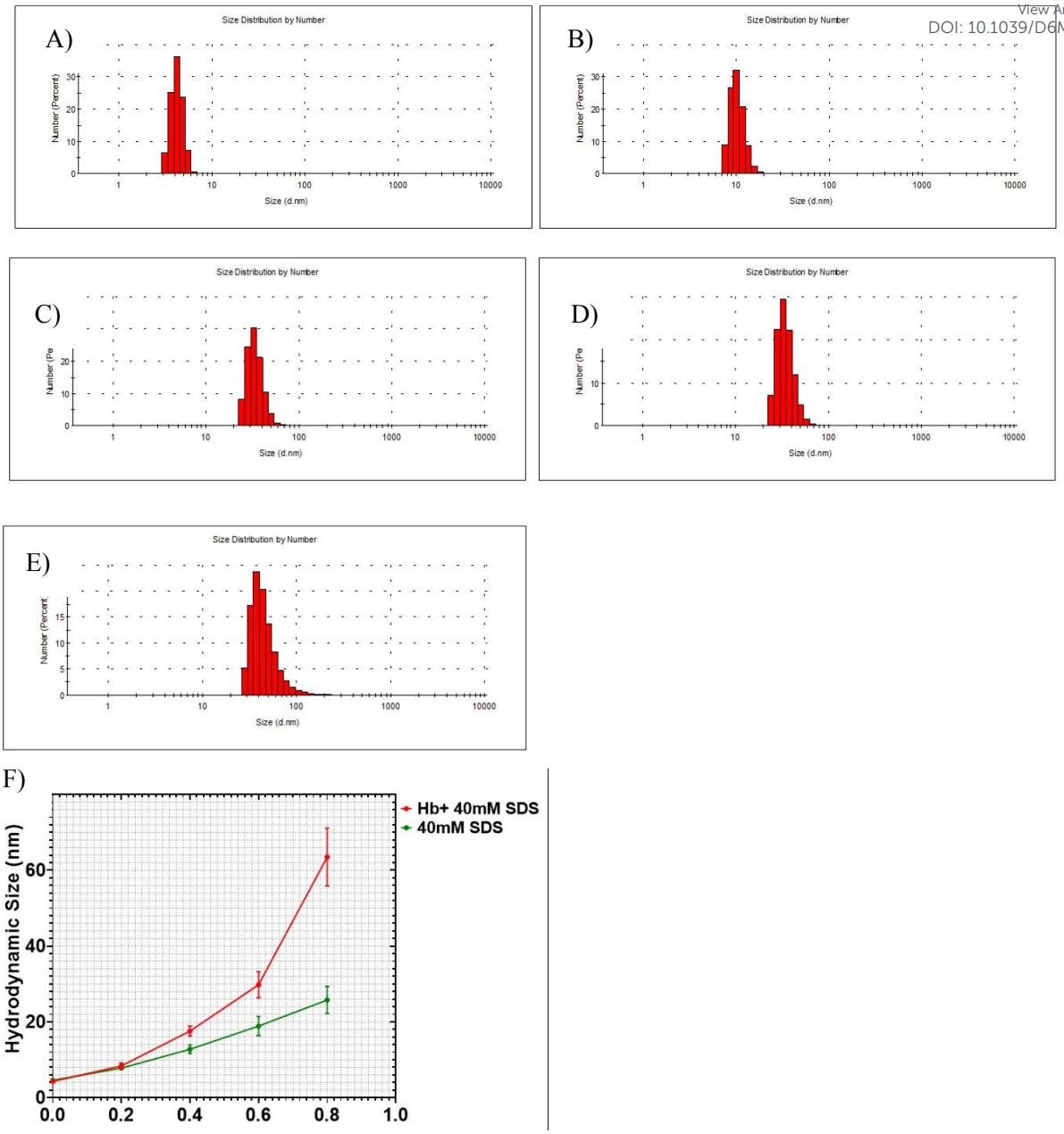

Figure 8. DLS analysis of SDS micelles and HbA_0-SDS complexes under varying ionic strength conditions. Representative size distribution profiles of HbA_0 (0.05 mg/mL) in the presence of 40 mM SDS at different NaCl concentrations (0-0.8 M) are shown, illustrating the progressive shift toward larger hydrodynamic sizes with increasing ionic strength. The distributions broaden and shift to higher size regimes at elevated salt concentrations, indicating increased heterogeneity and formation of larger assemblies. (A) 0M NaCl + 40mM SDS+ 0.05mg/mL Hb (B) 0.2M NaCl + 40mM SDS+ 0.05mg/mL Hb (C) 0.4M NaCl + 40mM SDS+ 0.05mg/mL Hb (D) 0.6M NaCl + 40mM SDS+ 0.05mg/mL Hb (A) 0.8 M NaCl + 40mM SDS+ 0.05mg/mL Hb (F)The corresponding plot summarizes the **hydrodynamic diameter (Dh)** of HbA_0–SDS complexes compared with SDS alone as a function of NaCl concentration. While

SDS micelles exhibit a gradual increase in size with increasing salt concentration. HbA_0–SDS systems show a significantly larger increase in Dh, rising from ~4.3 nm (0 M) to ~63 nm (0.8 M NaCl). This pronounced growth reflects enhanced protein–surfactant association and the formation of extended, anisotropic assemblies under electrostatic screening conditions.

All measurements were performed at 25 °C in buffer (pH 7.4), and data are presented as mean ± standard deviation (n = 3).

Table 5: Hydrodynamic diameter (Dh) of HbA_0 (0.05 mg/mL) with increasing SDS (0-80 mM) showing protein size reduction and micellar growth (mean ± SD, n = 3, 25 °C, pH 7.4).

Concentration of SDS (mM)	**0.05 mg/mL Hb + SDS Hydrodynamic Size (nm)**
0	6.50 ± 0.28
5	5.26 ±0.25
10	4.70 ± 0.40
20	4.30 ± 0.34
40	4.40 ± 0.27
80	4.53 ± 0.25

Table 6: Hydrodynamic diameter (Dh) of HbA_0 (0.05 mg/mL) + 40 mM SDS and SDS alone as a function of NaCl (0–0.8 M), showing salt-induced growth of protein–surfactant assemblies (mean ± SD, n = 3, 25 °C, pH 7.4).

Concentration of NaCl (M)	**0.05 mg/mL Hb + 40mM SDS Hydrodynamic Size (nm)**	**40mM SDS Hydrodynamic Size (nm)**
0	4.30 ± 0.27	4.60 ± 0.14
0.2	8.40 ± 0.76	7.80 ± 0.56

0.4	17.60 ± 1.34	12.80 ± 1.13
0.6	29.80 ± 3.40	18.90 ± 2.54
0.8	63.50 ± 7.60	25.80 ± 3.56

4. Discussion

The combined spectroscopic and SANS analyses provide a comprehensive mechanistic picture of how SDS modulates the structural organization of Hemoglobin A_0 (HbA_0) at both secondary and quaternary levels. Unlike globular single-chain proteins such as BSA or lysozyme, HbA_0 unfolds through a unique subunit-dissociation pathway due to its tetrameric architecture and the distinct distribution of electrostatic and hydrophobic contacts at the $\alpha_1\beta_2$ and $\alpha_2\beta_1$ interfaces [48,49]. Our findings establish that low concentrations (0-5mM) of SDS are sufficient to initiate dissociation of the tetrameric scaffold, highlighting the susceptibility of multimeric proteins to local surfactant interactions well before micelle formation.

UV-visible spectroscopy revealed progressive heme-pocket perturbation characterized by the disappearance of oxyhemoglobin bands (540 and 575 nm) and a Soret shift from 414 nm to ~408 nm, consistent with $Fe^{2+} \rightarrow Fe^{3+}$ oxidation and methemoglobin formation. This is accompanied by the emergence of the 395 nm band representing free heme, suggesting destabilization of the hydrophobic heme-binding cavity. Fluorescence measurements demonstrated disruption of Tyr→Trp energy transfer, with significant blue-shifting and intensity enhancement indicating exposure of previously buried aromatic residues. Together, these spectroscopic signatures point toward localized unfolding proximal to the heme pocket and destabilization of inter-subunit interfaces.

SANS provided structural information unattainable through spectroscopy alone. At low SDS concentrations (≤5 mM), the effective radius and Dmax decreased markedly, consistent with a transition from tetramers to dimers and monomers. The observed ~6-fold increase in scattering entities supports a model in which SDS monomers bind preferentially to positively charged interfacial patches at the α–β interfaces (Lys, Arg, His clusters) and insert hydrophobic tails into shallow pockets lining these regions. This specific, localized binding weakens native inter-subunit salt bridges and hydrophobic packing. Because these interfaces are less hydrophobically buried and structurally looser compared to those in other tetrameric proteins (e.g., lactate dehydrogenase), HbA_0 is particularly susceptible to dissociation. Importantly, the

heme pockets reside within individual subunits rather than at the interfaces, explaining why quaternary dissociation precedes global unfolding. This accounts for the sequential tetramer → dimer → monomer evolution detected by SANS.

CD spectroscopy corroborated this dissociation-first process: an initial loss of α-helicity is followed by partial recovery at higher SDS concentrations, coinciding with micelle formation. At higher concentrations (5-80mM), additional SDS does not further disrupt structure; instead, free micelles stabilize the already-dissociated monomers through surfactant–protein complexes, indicating saturation of the primary molecular binding sites.

The effects of ionic strength further illuminate the interplay between electrostatics and surfactant binding. The presence of NaCl amplifies SDS-induced dissociation and leads to extended rod-like complexes, as evidenced by increased axial anisotropy and larger Dmax values in SANS profiles. Charge screening by NaCl reduces repulsion among SDS-coated protein units, enabling linear aggregation into elongated morphologies. Notably, the non-monotonic response at 0.2 M versus 0.4 M NaCl highlights a balance between screened electrostatic repulsion, micelle growth, and complex co-assembly, emphasizing that ionic environment is a powerful determinant of protein–surfactant architecture [50].

The bright-field microscopy images provide complementary, real-space evidence for the concentration-dependent structural reorganization of HbA_0 in the presence of SDS. At low SDS concentrations (≤0.1 mM), the samples remain optically homogeneous, consistent with dispersed protein species and the early stages of subunit dissociation inferred from SANS. In contrast, at higher SDS concentrations (≥1 mM), pronounced dark, irregular aggregates become visible, indicating the emergence of larger, heterogeneous protein–surfactant assemblies and the coexistence of multiple structural species that are ensemble-averaged in SANS measurements. While these images do not resolve nanoscale elongated morphologies, they corroborate the onset of higher-order association and increasing heterogeneity with rising surfactant concentration. Direct imaging techniques such as TEM or AFM could, in principle, visualize elongated structures; however, SDS–protein assemblies are highly sensitive to drying, staining, and surface adsorption, which can disrupt their native hydrated morphology and introduce artifacts. The strong agreement between SANS-derived elongation and corroborating spectroscopic signatures further supports the structural interpretation presented.

The combined spectroscopic, SANS, and DLS analyses provide a comprehensive and internally consistent picture of the structural transitions of Hemoglobin A_0 (HbA_0) in the presence of SDS. Importantly, the integration of these complementary techniques allows us to resolve both local conformational changes and global structural reorganization across multiple

View Article Online
DOI: 10.1039/D6MA00049E

length scales. A key outcome of this study is the identification of a subunit-dissociation-driven pathway, rather than classical unfolding, as the dominant structural response of HbA_0 to SDS. Unlike single-chain globular proteins such as BSA, where surfactant-induced unfolding is typically associated with micellization and formation of extended polypeptide–micelle complexes, HbA_0 exhibits a fundamentally different behavior due to its tetrameric architecture. The spectroscopic data (UV–visible and fluorescence) reveal early perturbations in the heme environment and disruption of Tyr→Trp energy transfer at relatively low SDS concentrations. These changes are indicative of local structural rearrangements and increased solvent exposure of aromatic residues. More importantly, SANS and DLS provide direct structural evidence that these changes are accompanied by a reduction in particle size, consistent with the dissociation of tetrameric HbA_0 into smaller subunits. Specifically, the hydrodynamic diameter decreases from ~6.5 nm to ~4.3 nm (DLS), while SANS shows a corresponding reduction in effective radius and D_{max} (SANS) confirm that structural transitions occur at very low concentration (0-5mM) of SDS.

While SDS is structurally heterogeneous (including premicellar aggregates), our results show that interactions between SDS (monomers/small aggregates) and protein subunit interfaces drive dissociation independent of bulk micelles, meaning multimeric protein responses cannot be explained solely by micellization thresholds. SDS is not purely monomeric below the CMC and is influenced by protein and ionic conditions; DLS of SDS alone shows gradual size increases with concentration and salt. However, HbA_0–SDS shows initial size reduction then stabilization, indicating protein–surfactant interactions dominate early transitions. Thus, SDS in multiple aggregation states destabilizes HbA_0 quaternary structure. Increasing ionic strength amplifies this effect: size rises to ~63 nm (with higher Dmax and anisotropy in SANS), far exceeding SDS micelles alone (~25–26 nm), showing electrostatic screening promotes protein–surfactant co-assembly into larger, anisotropic, worm-like structures.

Importantly, these results provide insight into the longstanding question of whether SDS-induced protein destabilization is governed primarily by micelle formation or monomer binding. In HbA_0, the principal structural transitions occur well below the CMC, showing conclusively that SDS monomer snot micelles drive the dissociation mechanism. This distinguishes HbA_0 from single-chain proteins like BSA, where unfolding correlates strongly with micellization.

View Article Online
DOI: 10.1039/D6MA00049E

From a materials perspective, these mechanistic findings have significant implications. Protein-based formulations, Hemoglobin-loaded nanocarriers, membrane-immobilized sensors, and Hemoglobin-inspired biomaterials all rely on maintaining quaternary stability. The finding that SDS triggers dissociation at sub-millimolar levels underscores the need for careful control of surfactant content, ionic strength, and interface chemistry during fabrication. Moreover, the formation of extended structures under salt-rich conditions suggests possible strategies for engineering anisotropic protein–surfactant assemblies for biomaterial or nanostructure applications. By mapping the dissociation pathway and identifying the structural states accessible under controlled solution conditions, this study provides a mechanistic framework that is highly relevant to both biological and materials-processing environments.

5. Conclusions and Future outlook

In summary, this work delineates the stepwise structural evolution of Hemoglobin A_0 in the presence of the anionic surfactant SDS, integrating spectroscopic and microscopic analyses with SANS to resolve transitions from the native tetramer to dimeric and monomeric units. Our results demonstrate that SDS induces dissociation at concentrations far below the CMC, driven by specific monomer–protein interactions rather than bulk micellization. This subunit-level destabilization occurs because SDS binds to distinct electrostatic and hydrophobic patches at the α–β interfaces, weakening quaternary contacts and promoting dissociation prior to any major changes in secondary structure.

The presence of electrolytes further modulates these interactions, promoting the formation of extended worm-like assemblies through electrostatic screening and enhanced surfactant–protein association. This behavior contrasts sharply with classical systems such as BSA or lysozyme, where unfolding is governed largely by CAC/CMC-dependent micellization. For multimeric proteins such as HbA_0, the CAC or CMC are not the dominant factors determining the unfolding pathway; instead, molecular-level binding of SDS monomers dictates the dissociation mechanism. Excess SDS beyond the saturation point remains as free micelles, contributing to colloidal stability through increased electrostatic repulsion rather than driving additional unfolding.

Although our results show clear differences in HbA_0 behavior below and above the CMC, the crucial distinction lies in the underlying mechanism rather than in the relevance of the CMC itself. For HbA_0, the primary structural transition tetramer dissociation into dimers and monomers—occurs well below the CMC and is initiated by SDS monomer binding at inter-subunit interfaces. Above the CMC, additional micelles do not induce further unfolding but instead stabilize the already-dissociated subunits. This behavior contrasts with proteins such as

View Article Online
DOI: 10.1039/D6MA00049E

BSA or lysozyme, where unfolding or aggregation corresponds strongly to CAC/CMC-dependent micellization.

These mechanistic insights extend well beyond fundamental biophysical chemistry and are directly relevant to the design and stability of protein-containing materials. Understanding how surfactants drive quaternary destabilization provides a framework for improving the robustness of hemoglobin-based oxygen carriers, optimizing protein encapsulation within nanocarriers, preventing aggregation during materials processing, and preserving structural integrity when immobilizing hemoglobin in biosensor platforms. The structural transitions mapped here offer practical guidance for engineering stable protein–material hybrids and anticipating surfactant-mediated effects in formulation environments.

Future work exploring the role of multivalent ions, alternative surfactant architectures, or polymer surfactant co-assemblies may further refine control over protein structural states. Such studies will deepen understanding of protein surfactant interactions in complex materials and support the rational design of next-generation protein-based technologies.

Acknowledgements

D.S. wishes to thank the Department of Science and Technology (DST), India, for the grant (DST/INSPIRE/04/2015/003265). JB also likes to thank Department of Science and Technology (DST) for the grant TDP/BDTD/25/2019, Indian Council of Medical Research (ICMR) for the grant (2020-2982), University Grants Commission, India, the Department of Biotechnology (Project No.: BT/PR49857/MED/32/850/2023), the Indian Council of Medical Research (Project No.: EM/DEV/SG/149/2497/2023), ANRF PAIR (File No.: ANRF/PAIR/2025/000029/PAIR-A (G)), and the UGC Faculty Recharge Programme for funding support.HG also likes to thank Ministry of Education, Government of India for providing financial support in the form of Prime Minister's Research Fellowship.

Declaration of competing interest

The authors declare that they have no known competing financial interests or personal relationships that could have appeared to influence the work reported in this paper.

Author Contributions

Debasish Saha: Methodology, Validation, Investigation, Formal Analysis, Writing-original draft,Resources. **Suhail Khan:** Methodology, Investigation, Formal Analysis **Harsh A. Gandhi:** Methodology, Validation, Investigation, Formal Analysis, Writing- original

View Article Online
DOI: 10.1039/D6MA00049E

draft**Shafinaz Rahman Sarah:** Investigation,Writing- review & editing **Vinod Kumar Aswal:** Methodology, Formal Analysis, Resources. **Jaydeep Bhattacharya:** Conceptualization, Validation, Methodology, Formal Analysis, Supervision, Writing -review & editing, Funding acquisition, Resources.

References

[1] M.N. Jones, Surfactant interactions with biomembranes and proteins, Chem Soc Rev. 21 (1992) 127–136. https://doi.org/10.1039/CS9922100127.

[2] D. Otzen, Protein–surfactant interactions: A tale of many states, Biochim. Biophys. Acta. 1814 (2011) 562–591. https://doi.org/10.1016/j.bbapap.2011.03.003.

[3] N. El Kadi, N. Taulier, J.Y. Le Huérou, M. Gindre, W. Urbach, I. Nwigwe, P.C. Kahn, M. Waks, Unfolding and Refolding of Bovine Serum Albumin at Acid pH: Ultrasound and Structural Studies, Biophys. J. 91 (2006) 3397–3404. https://doi.org/10.1529/biophysj.106.088963.

[4] C. Sun, J. Yang, X. Wu, X. Huang, F. Wang, S. Liu, Unfolding and Refolding of Bovine Serum Albumin Induced by Cetylpyridinium Bromide, Biophys. J. 88 (2005) 3518–3524. https://doi.org/10.1529/biophysj.104.051516.

[5] A. Riccio, L. Vitagliano, G. di Prisco, A. Zagari, L. Mazzarella, The crystal structure of a tetrameric hemoglobin in a partial hemichrome state, Proc. Natl. Acad. Sci. 99 (2002) 9801. https://doi.org/10.1073/pnas.132182099.

[6] D. Rutkowska-Zbik, M. Witko, G. Stochel, Theoretical density functional theory studies on interactions of small biologically active molecules with isolated heme group, J. Comput. Chem. 28 (2007) 825–831. https://doi.org/10.1002/jcc.20598.

[7] M.F. PERUTZ, Stereochemistry of Cooperative Effects in Haemoglobin: Haem–Haem Interaction and the Problem of Allostery, Nature. 228 (1970) 726–734. https://doi.org/10.1038/228726a0.

[8] Y. Wang, R. Guo, J. Xi, Comparative studies of interactions of hemoglobin with single-chain and with gemini surfactants, J. Colloid Interface Sci. 331 (2009) 470–475. https://doi.org/10.1016/j.jcis.2008.12.020.

[9] F.A.O. Carvalho, J.W.P. Carvalho, E. Biazin, P.S. Santiago, M. Tabak, Characterization of Rhinodrilus alatus hemoglobin (HbRa) and its subunits: Evidence for strong interaction with cationic surfactants DTAB and CTAC, Comp. Biochem. Physiol. B Biochem. Mol. Biol. 167 (2014) 23–29. https://doi.org/10.1016/j.cbpb.2013.09.007.

[10] M. Akram, S. Anwar, I.A. Bhat, Kabir-ud-Din, In vitro evaluation of the non-covalent interactions of hemoglobin with distinctively modified gemini surfactants: Effect of structural variation, Colloids Surf. Physicochem. Eng. Asp. 527 (2017) 145–157. https://doi.org/10.1016/j.colsurfa.2017.05.021.

[11] H. Sun, H. Ma, N. Hu, Electroactive hemoglobin–surfactant–polymer biomembrane-like films, Bioelectrochem. Bioenerg. 49 (1999) 1–10. https://doi.org/10.1016/S0302-4598(99)00060-4.

[12] P.S. Santiago, L.M. Moreira, E.V. de Almeida, M. Tabak, Giant extracellular GlossoscolexpaulistusHemoglobin (HbGp) upon interaction with cethyltrimethylammonium chloride (CTAC) and sodium dodecyl sulphate (SDS) surfactants: Dissociation of oligomeric structure and autoxidation, Biochim. Biophys. Acta, 1770 (2007) 506–517. https://doi.org/10.1016/j.bbagen.2006.11.005.

[13] P.S. Santiago, F.A.O. Carvalho, M.M. Domingues, J.W.P. Carvalho, N.C. Santos, M. Tabak, Isoelectric Point Determination for Glossoscolexpaulistus Extracellular Hemoglobin: Oligomeric Stability in Acidic pH and Relevance to Protein−Surfactant Interactions, Langmuir. 26 (2010) 9794–9801. https://doi.org/10.1021/la100060p.

[14] R. Vashishat, S. Chabba, R.K. Mahajan, Surface active ionic liquid induced conformational transition in aqueous medium of hemoglobin, RSC Adv. 7 (2017) 13041–13052. https://doi.org/10.1039/C7RA00075H.

[15] A.A. Rafati, E. Ghasemian, Thermodynamic and binding study of hemoglobin, oxy-hemoglobin and carbamino-hemoglobin upon interaction with cationic surfactants, using surfactant membrane selective electrodes, J. Mol. Liq. 144 (2009) 131–137. https://doi.org/10.1016/j.molliq.2008.10.010.

[16] D.E. Otzen, Protein unfolding in detergents: effect of micelle structure, ionic strength, pH, and temperature, Biophys. J. 83 (2002) 2219–2230.

[17] K.K. Andersen, C.L. Oliveira, K.L. Larsen, F.M. Poulsen, T.H. Callisen, P. Westh, J.S. Pedersen, D. Otzen, The Role of Decorated SDS Micelles in Sub-CMC Protein Denaturation and Association, J. Mol. Biol. 391 (2009) 207–226. https://doi.org/10.1016/j.jmb.2009.06.019.

[18] S. Chodankar, V.K. Aswal, J. Kohlbrecher, R. Vavrin, A.G. Wagh, Surfactant-induced protein unfolding as studied by small-angle neutron scattering and dynamic light scattering, J. Phys. Condens. Matter. 19 (2007) 326102. https://doi:10.1088/0953-8984/19/32/326102.

[19] S. Chodankar, V.K. Aswal, P.A. Hassan, A.G. Wagh, Structure of protein–surfactant complexes as studied by small-angle neutron scattering and dynamic light scattering, Phys. B Condens. Matter. 398 (2007) 112–117. https://doi.org/10.1016/j.physb.2007.05.003.

[20] S. Mehan, V.K. Aswal, J. Kohlbrecher, Tuning of protein-surfactant interaction to modify the resultant structure, Phys Rev E. 92 (2015) 32713. https://doi.org/10.1103/PhysRevE.92.032713.

[21] D. Saha, D. Ray, S. Kumar, J. Kohlbrecher, V.K. Aswal, Interaction of a bovine serum albumin (BSA) protein with mixed anionic–cationic surfactants and the resultant structure, Soft Matter. 17 (2021) 6972–6984. https://doi.org/10.1039/D1SM00264C.

[22] S. Hayashi, S. Ikeda, Micelle size and shape of sodium dodecyl sulfate in concentrated sodium chloride solutions, J. Phys. Chem. 84 (1980) 744–751. https://doi.org/10.1021/j100444a011.

[23] S. Kumar, D. Saha, D. Ray, S. Abbas, V.K. Aswal, Unusual stability of protein molecules in the presence of multivalent counterions, Phys. Rev. E. 104 (2021) L012603. https://doi.org/10.1103/PhysRevE.104.L012603.

[24] J.M. Hempe, R.D. Craver, Separation of hemoglobin variants with similar charge by capillary isoelectric focusing: Value of isoelectric point for identification of common and uncommon hemoglobin variants, ELECTROPHORESIS. 21 (2000) 743–748. https://doi.org/10.1002/(SICI)1522-2683(20000301)21:4<743::AID-ELPS743>3.0.CO;2-1.

[25] V.K. Aswal, P.S. Goyal, Small-angle neutron scattering diffractometer at Dhruva reactor, Curr. Sci. 79 (2000) 947–953.

[26] I. Breßler, J. Kohlbrecher, A.F. Thünemann, SASfit: a tool for small-angle scattering data analysis using a library of analytical expressions, J. Appl. Crystallogr. 48 (2015) 1587–1598. https://doi.org/10.1107/S1600576715016544.

[27] J.B. Hayter, J. Penfold, Determination of micelle structure and charge by neutron small-angle scattering, Colloid Polym. Sci. 261 (1983) 1022–1030. https://doi.org/10.1007/BF01421709.

[28]C.A. Dreiss, Wormlike micelles: where do we stand? Recent developments, linear rheology and scattering techniques, Soft Matter 3 (2007) 956–970. https://doi.org/10.1039/B705775J.

[29] D.I. Svergun, M.H.J. Koch, Small-angle scattering studies of biological macromolecules in solution, Rep. Prog. Phys. 66 (2003) 1735.

[30] S.B. Brown, M. Shillcock, P. Jones, Equilibrium and kinetic studies of the aggregation of porphyrins in aqueous solution, Biochem. J. 153 (1976) 279–285. https://doi.org/10.1042/bj1530279.

[31] S. Mondal, A. Banerjee, B. Das, Spectroscopic and interfacial investigation on the interaction of hemoglobin with conventional and ionic liquid surfactants, J. Mol. Liq. 301 (2020) 112450. https://doi.org/10.1016/j.molliq.2020.112450.

[32] A. Mavani, A. Ovung, S. Luikham, G. Suresh Kumar, A. Das, D. Ray, V.K. Aswal, J. Bhattacharyya, Biophysical and molecular modeling evidences for the binding of sulfa molecules with hemoglobin, J. Biomol. Struct. Dyn. (2022) 1–12. https://doi.org/10.1080/07391102.2022.2057358.

[33] B.L. Tekwani, L.A. Walker, Targeting the hemozoin synthesis pathway for new antimalarial drug discovery: technologies for in vitro beta-hematin formation assay, Comb. Chem. High Throughput Screen. 8 (2005) 63–79. https://doi.org/10.2174/1386207053328101.

[34] A.V. Graça-Souza, C. Maya-Monteiro, G.O. Paiva-Silva, G.R.C. Braz, M.C. Paes, M.H.F. Sorgine, M.F. Oliveira, P.L. Oliveira, Adaptations against heme toxicity in blood-feeding arthropods., Insect Biochem. Mol. Biol. 36 (2006) 322–335. https://doi.org/10.1016/j.ibmb.2006.01.009.

[35] C.J. Coates, H. Decker, Immunological properties of oxygen-transport proteins: hemoglobin, hemocyanin and hemerythrin, Cell. Mol. Life Sci. 74 (2017) 293–317. https://doi.org/10.1007/s00018-016-2326-7.

[36] K. Manalastas-Cantos, P.V. Konarev, N.R. Hajizadeh, A.G. Kikhney, M.V. Petoukhov, D.S. Molodenskiy, A. Panjkovich, H.D.T. Mertens, A. Gruzinov, C. Borges, C.M. Jeffries, D.I. Svergun, D. Franke, ıt ATSAS 3.0: expanded functionality and new tools for small-angle scattering data analysis, J. Appl. Crystallogr. 54 (2021) 343–355. https://doi.org/10.1107/S1600576720013412.

[37] J. Schelten, P. Schlecht, W. Schmatz, A. Mayer, Neutron small angle scattering of hemoglobin., J. Biol. Chem. 247 (1972) 5436–5441.

[38] A.M. Stadler, R. Schweins, G. Zaccai, P. Lindner, Observation of a Large-Scale Superstructure in Concentrated Hemoglobin Solutions by Using Small Angle Neutron Scattering, J. Phys. Chem. Lett. 1 (2010) 1805–1808. https://doi.org/10.1021/jz100576c.

[39] J.S. Pedersen, Analysis of small-angle scattering data from colloids and polymer solutions: modeling and least-squares fitting, Adv. Colloid Interface Sci. 70 (1997) 171–210. https://doi.org/10.1016/S0001-8686 (97)00312-6.

[40] J.B. Hayter, J. Penfold, An analytic structure factor for macroion solutions, Mol. Phys. 42 (1981) 109–118. https://doi.org/10.1080/00268978100100091.

[41] E. Dutkiewicz, A. Jakubowska, Effect of electrolytes on the physicochemical behaviour of sodium dodecyl sulphate micelles, Colloid Polym. Sci. 280 (2002) 1009–1014. https://doi.org/10.1007/s00396-002-0723-y.

[42] D. Saha, D. Ray, J. Kohlbrecher, V.K. Aswal, Unfolding and Refolding of Protein by a Combination of Ionic and Nonionic Surfactants, ACS Omega. 3 (2018) 8260–8270. https://doi.org/10.1021/acsomega.8b00630.

[43] D. Saha, D. Ray, J. Kohlbrecher, V.K. Aswal, Random flight model analysis of protein-surfactant complexes, AIP Conf. Proc. 2115 (2019) 30033. https://doi.org/10.1063/1.5112872.

[44] Y.-X. Huang, Z.-J. Wu, B.-T. Huang, M. Luo, Pathway and Mechanism of pH Dependent Human Hemoglobin Tetramer-Dimer-Monomer Dissociations, PLOS ONE. 8 (2013) e81708. https://doi.org/10.1371/journal.pone.0081708.

[45] J.B. Hayter, J. Penfold, An analytic structure factor for macroion solutions, Mol. Phys. 42 (1981) 109–118. https://doi.org/10.1080/00268978100100091.

[46] J. Bhattacharyya, M. Bhattacharyya, A.S. Chakraborti, U. Chaudhuri, R.K. Poddar, Structural organisations of hemoglobin and myoglobin influence their binding behaviour with phenothiazines, Int. J. Biol. Macromol. 23 (1998) 11–18. https://doi.org/10.1016/S0141-8130 (98)00006-3.

[47] D. Arosio, H.E. Kwansa, H. Gering, G. Piszczek, E. Bucci, Static and dynamic light scattering approach to the hydration of hemoglobin and its supertetramers in the presence of osmolites, Biopolymers 63 (2002) 1–11. https://doi.org/10.1002/bip.1057.

[48] S. Kumar, D. Saha, S. Takata, V.K. Aswal, H. Seto, Modifications in the nanoparticle-protein interactions for tuning the protein adsorption and controlling the stability of complexes, Appl. Phys. Lett. 118 (2021) 153701. https://doi.org/10.1063/5.0046745.

[49] D. Saha, S. Kumar, D. Ray, J.P. Mata, A.E. Whitten, V.K. Aswal, Tuning of silica nanoparticle–lysozyme protein complexes in the presence of the SDS surfactant, Soft Matter. 18 (2022) 434–445. https://doi.org/10.1039/D1SM01340H.

[50] S. Kumar, D. Saha, D. Ray, V.K. Aswal, Surfactant-driven modifications in protein structure, Soft Matter 21 (2025) 4979–4998. https://doi.org/10.1039/D5SM00207A.

View Article Online
DOI: 10.1039/D6MA00049E

Data Availability Statement

Data will be made available on request.